PHYSICAL REVIEW A **91**, 031402(R) (2015)

Strong-field ionization with two-color circularly polarized laser fields

Christopher A. Mancuso,[1] Daniel D. Hickstein,[1,*] Patrik Grychtol,[1] Ronny Knut,[1] Ofer Kfir,[2] Xiao-Min Tong,[3] Franklin Dollar,[1] Dmitriy Zusin,[1] Maithreyi Gopalakrishnan,[1] Christian Gentry,[1] Emrah Turgut,[1] Jennifer L. Ellis,[1] Ming-Chang Chen,[4] Avner Fleischer,[2,5] Oren Cohen,[2] Henry C. Kapteyn,[1] and Margaret M. Murnane[1]

[1]*JILA and Department of Physics, University of Colorado Boulder and NIST, Boulder, Colorado 80309, USA*

[2]*Solid State Institute and Physics Department, Technion, Haifa, 32000, Israel*

[3]*Division of Material Science, Faculty of Pure and Applied Science, University of Tsukuba, Ibaraki 305-8573, Japan*

[4]*Institute of Photonics Technologies, National Tsing Hua University, Hsinchu 30013, Taiwan*

[5]*Department of Physics and Optical Engineering, Ort Braude College, Karmiel 21982, Israel*

(Received 21 November 2014; revised manuscript received 21 January 2015; published 25 March 2015)

Strong-field ionization provides fundamental insight into light-matter interactions, encoding the structure of atoms and molecules on the subångström and subfemtosecond scales. In this Rapid Communication, we explore an important regime: strong-field ionization by two-color circularly polarized laser fields. In contrast to past work using linearly polarized drivers, we probe electron trajectories that are driven in a two-dimensional plane, thus separating the tunneling angle from the rescattering angle. This allows us to make several findings. First, we observe a single-lobed electron distribution for co-rotating fields, and a three-lobed distribution for counter-rotating fields, providing experimental validation of the theoretical model explaining the generation of circularly polarized high harmonic light. Second, we discover that there is significant electron-ion rescattering using counter-rotating fields, but not with co-rotating fields. Finally, we show that the rescattered electrons are well separated from the directly ionized electrons, in striking contrast to similar low-energy structures seen with linearly polarized fields. These findings help overcome the long-standing problem of how to decouple the tunneling and rescattering steps in strong-field ionization, which will enable new dynamic probes of atomic and molecular structure.

DOI: 10.1103/PhysRevA.91.031402 PACS number(s): 32.80.Fb, 34.80.Qb, 42.65.Ky

The interaction of intense laser fields (10^{14} W cm^{-2}) with atoms and molecules is of great scientific and technological interest because of two related phenomena: high-harmonic generation (HHG) [1] and strong-field ionization (SFI) [2,3]. HHG enables tabletop generation of coherent beams of extreme ultraviolet (EUV) and soft x-ray light [4], which have a broad range of applications. For example, HHG makes it possible to capture chemical reactions in real time [5–7], to uncover correlated charge, spin, and phonon dynamics in materials with elemental specificity [8–10], and to perform coherent imaging on the nanometer scale near the wavelength limit [11,12]. Similarly, recent studies have revealed that the photoelectron distribution from SFI can provide information about the dynamic orbital and molecular structure [13–16], indicating its potential for understanding molecular dynamics.

Both HHG and SFI begin with the tunnel ionization of an electron from an atom or molecule, after which the free electron is accelerated in the laser field [17]. HHG occurs when an electron that is driven back to the parent ion recombines, releasing its kinetic energy by emitting a high-energy photon. SFI results from electrons that do not recombine, but may still re-encounter their parent ion and rescatter. The fact that both recombination (i.e., HHG) and rescattering are strongly suppressed in elliptically or circularly polarized driving laser fields [3,18–21] means that past studies have generally used linearly polarized light to drive the HHG and SFI processes. However, when using linearly polarized light, field-driven electrons are confined to one-dimensional (1D) trajectories, making it difficult to deconvolve molecular structural information encoded by both the tunnel-ionization and rescattering steps [22–24]. In contrast, using two-color circularly polarized fields, electrons are driven in a two-dimensional (2D) plane [25], allowing the tunneling and rescattering processes to occur at different angles.

In this Rapid Communication, we present several important experimental observations of SFI driven by two-color circularly polarized fields. First, the photoelectron distributions exhibit unusual symmetries: namely, a single-lobe crescent shape when the two fields have the same helicity (co-rotating), or a three-lobe shape when the fields have opposite helicity (counter-rotating). Second, low-energy features appear in the photoelectron distribution only when the two laser fields are counter-rotating. Advanced numerical calculations using the time-dependent Schrödinger equation show that these features are due to strong electron-ion rescattering. Finally, we observe that the low-energy rescattered electrons are well separated from those that do not re-encounter the core [3,26–30]. This demonstration of well-separated electron-ion rescattering structures paves the way for the development of spectroscopies that will steer the 2D electron trajectories (by adjusting intensities, frequencies, and ellipticities of the driving fields) in order to provide new probes of atomic and molecular dynamics.

In addition, the observation of the shape and symmetry of the photoelectron distributions resulting from two-color circularly polarized fields provides experimental validation of the theoretical model of HHG under these fields [25,31–35]. Recently, HHG driven by counter-rotating fields has been demonstrated as a breakthrough source of coherent circularly polarized EUV light, enabling powerful spectroscopies—such

*Corresponding author: danhickstein@gmail.com

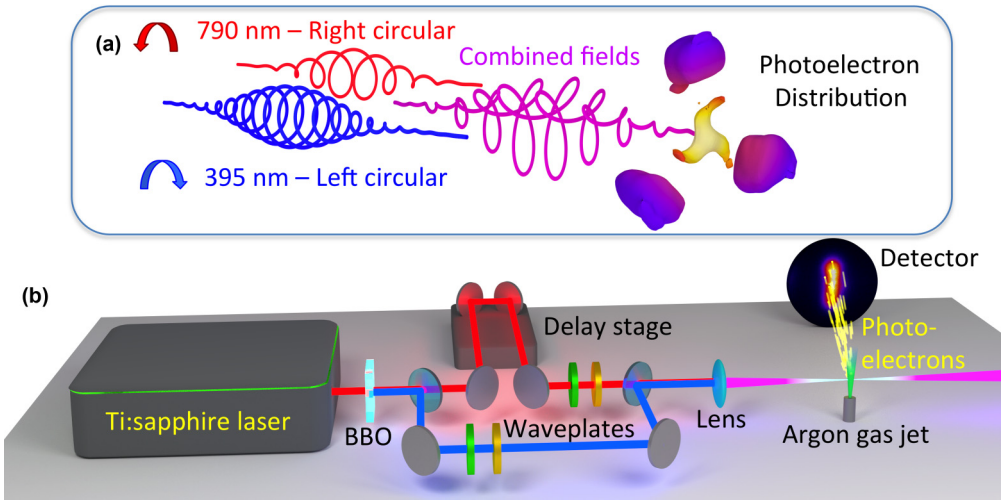

FIG. 1. (Color online) (a) Two-color counter-rotating circularly polarized laser fields ionize atoms to produce photoelectron distributions that exhibit distinct features (central yellow lobes) that result from electron-ion rescattering. (b) Experimental apparatus used to detect the photoelectron distributions.

as probing chiral molecules using photoelectron circular dichroism [36,37] and investigating femtosecond magnetic dynamics using x-ray magnetic circular dichroism [34,38]—to move from the synchrotron to the tabletop. The theoretical model for HHG under these conditions is built on the idea that electrons can be driven back to the parent ion three times per laser cycle, each time at a different angle. Our observation of threefold symmetric photoelectron distributions provides direct experimental validation of this elegant theoretical model.

To study SFI with two-color circularly polarized fields, we used a velocity map imaging (VMI) spectrometer [39] to record 2D projections of the three-dimensional (3D) photoelectron distributions onto a microchannel-plate–phosphor-screen detector (Beam Imaging Solutions) and a CCD camera (Fig. 1). The fundamental laser pulses (790 nm, 45 fs) were derived from a Ti:sapphire regenerative laser amplifier (KMLabs Wyvern HP) operating at 4 kHz. The second harmonic (395 nm) was obtained via frequency doubling in a 200-μm-thick beta barium borate (BBO) crystal. Dichroic mirrors were used to separate, and later recombine, the fundamental and second harmonic in a Mach–Zehnder geometry. A delay stage was placed in the 790 nm arm to control the relative time delay of the laser pulses. Waveplates ($\lambda/4$ and $\lambda/2$) were placed in each beam to separately control the polarization of the 395-nm and 790-nm laser pulses. A one-to-one magnification telescope consisting of two lenses was placed in the 790-nm arm of the delay line to compensate for chromatic aberration in the final focusing lens. The laser pulses were focused into a skimmed supersonic jet of argon gas, with intensities of $\sim 5 \times 10^{13}$ W cm^{-2} for each of the beams separately. The photoelectron distributions were then recorded as a function of the time delay between the fundamental and the second harmonic, using a step size of $\sim$133 attoseconds. The experiment was carried out by combining the fundamental and second harmonic fields in two distinct cases: with the fields counter-rotating, and with the fields co-rotating.

By recording the photoelectron distributions as a function of time delay between the 395-nm and 790-nm fields, we make several important discoveries about SFI under two-color circularly polarized fields: (1) The shape of the photoelectron distributions depends on the relative helicities between the circularly polarized fields. (2) The electron distributions rotate with the time delay between the two laser fields, allowing the 3D photoelectron distribution to be reconstructed using tomographic methods [40–43]. (3) Counter-rotating fields enable electron-ion rescattering (and HHG), which is not present for co-rotating fields.

One noticeable difference in the shape of the photoelectron distribution between the two cases is that the co-rotating circular fields produce higher kinetic energy photoelectrons than the counter-rotating fields. The differences in the photoelectron kinetic energies can be explained through a simple analysis of the electric field ($\vec{E}$) that results from the sum of the two laser fields. Within the strong-field approximation (SFA), which ignores the role of the Coulomb potential of the ion, the final drift momentum of the electron is given by $\vec{p}(t_b) = (p_x, p_y) = \int_{t_b}^{\infty} \vec{E}(t)dt$, where t_b is the time that the electron tunnels from the atom. To predict the photoelectron distributions, two factors must be considered: $\vec{p}\,(t_b)$, which is where an electron that tunnels at t_b will impact on the spectrometer, and $\vec{E}$, which determines the probability that an electron will tunnel ionize at that moment, and therefore the signal intensity on the spectrometer.

In the case of counter-rotating fields, the total electric field vector traces out a trefoil or "three-leaf clover" pattern [Fig. 2(a)], which has three maxima per laser cycle. These three maxima in E correspond to the three minima in final momentum p, which leads to the expectation that the photoelectron distribution from counter-rotating fields should consist of three lobes separated by 120°. In contrast, for the case of co-rotating fields, the electric field has only a single maximum per laser cycle [Fig. 2(b)], and this maximum in E corresponds to a maximum in p. Thus, co-rotating circularly polarized pulses should produce a photoelectron distribution that consists of a single lobe of relatively high kinetic energy electrons. Thus, the most prominent differences in the photoelectron kinetic energies from co- and counter-rotating circularly polarized fields can be explained as a result of electrons that tunnel

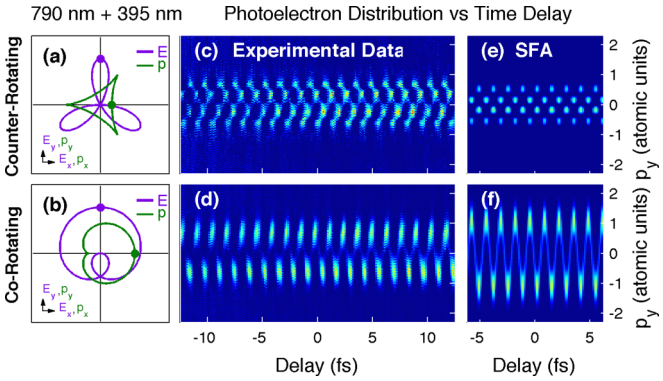

FIG. 2. (Color online) (a),(b) The combined laser electric field ($\vec{E}$) and final drift momentum of tunnel-ionized electrons ($\vec{p}$), where the dots indicate time zero for $\vec{E}$ and $\vec{p}$. (c),(d) Normalized 1D projections of the experimental photoelectron distributions plotted as a function of time delay between the 790-nm and 390-nm laser pulses, which reveal oscillations due to the rotation of the photoelectron distribution with a period of 1.3 fs (one cycle of the 395-nm field). (e),(f) Theoretical photoelectron distributions using the strong-field approximation (SFA) reproduce the qualitative differences between the co-rotating and counter-rotating cases.

ionize near the peak of the two-color laser field and proceed to the detector without re-encountering the parent ion.

To determine the role of electron-ion rescattering in SFI from two-color circularly polarized laser fields, it is necessary to evaluate the complete 3D photoelectron distribution. However, the VMI spectrometer only records a 2D projection on the detector, and the lack of cylindrical symmetry prevents conventional reconstruction techniques [44]. Since the laser propagation direction (z axis) is parallel to the detector, the plane that contains the 2D electric field created by the two-color circularly polarized field is perpendicular to the detector. This means that the VMI spectrometer can only collect information in one dimension of the laser field (y axis), whereas information in the other dimension (x axis) cannot be directly obtained.

Fortunately, one of the unique aspects of circularly polarized laser fields produced by combining the fundamental and second harmonic fields is that the electric field distribution can be rotated in the laboratory frame simply by changing the time delay between the two laser pulses [45]. Normalized sinograms were created through three data processing steps. First, each time-delay step was averaged over the laser propagation direction. Second, in order to compensate for changes in the total photoelectron yield due to the cross correlation of the laser pulses, each time step is divided by its mean value. Finally, the non-rotating component of the distributions consisting of electrons generated in regions where the pulses do not overlap was subtracted out to better highlight the oscillatory features of the distributions.

These normalized sinograms show that for counter-rotating fields [Fig. 2(c)], the three-lobed distribution rotates 120° in one cycle of the second harmonic (1.3 fs). For co-rotating fields [Fig. 2(d)], the single-lobed distribution makes one full revolution for every cycle of the second harmonic. In both cases, the photoelectron distribution returns to a point of

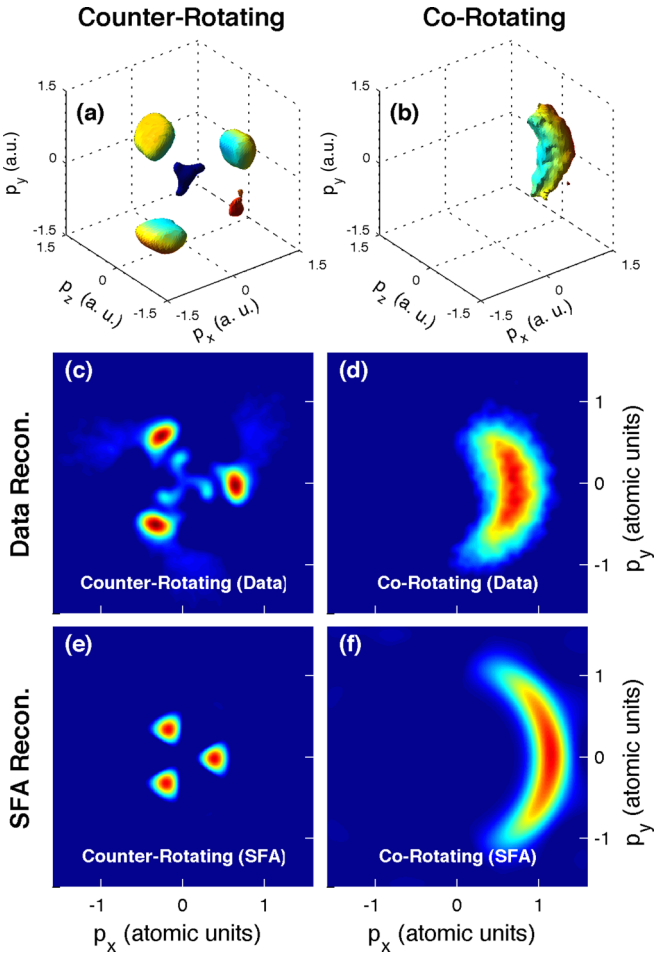

FIG. 3. (Color online) (a),(b) The experimental 3D photoelectron distribution for both counter- and co-rotating fields. (c)–(f) 2D projections of the 3D photoelectron distribution are compared to 2D SFA calculations. While the co-rotating data (d) is adequately reproduced by the SFA calculations (f), the counter-rotating case (c) exhibits low-energy structures that do not appear in the SFA model (e).

symmetry every 1.3 fs, as is seen in the experimental data [Figs. 2(c) and 2(d)]. These oscillating distributions can be modeled by weighting the final drift momentum by the tunnel-ionization rate [29] over a number of different relative time delays of the two laser pulses [Figs. 2(e) and 2(f)]. This ability to arbitrarily rotate the photoelectron distribution allows for the reconstruction of the 3D photoelectron distribution using tomographic reconstruction techniques [40–43]. By applying the inverse Radon transform [46] to each slice in the laser propagation (z) direction, a complete 3D reconstruction of the photoelectron distribution is obtained [Figs. 3(a) and 3(b)]. The photoelectron distribution resulting from the counter-rotating case manifests as a three-lobed shape with significant electron density near zero kinetic energy.

By examining 2D projections of the 3D photoelectron distributions, we can easily observe additional features that are indicative of the continuum dynamics of laser driven electrons. We compare the experimental photoelectron distributions [Figs. 3(c) and 3(d)] with the distributions predicted using the SFA [Figs. 3(e) and 3(f)], which ignores

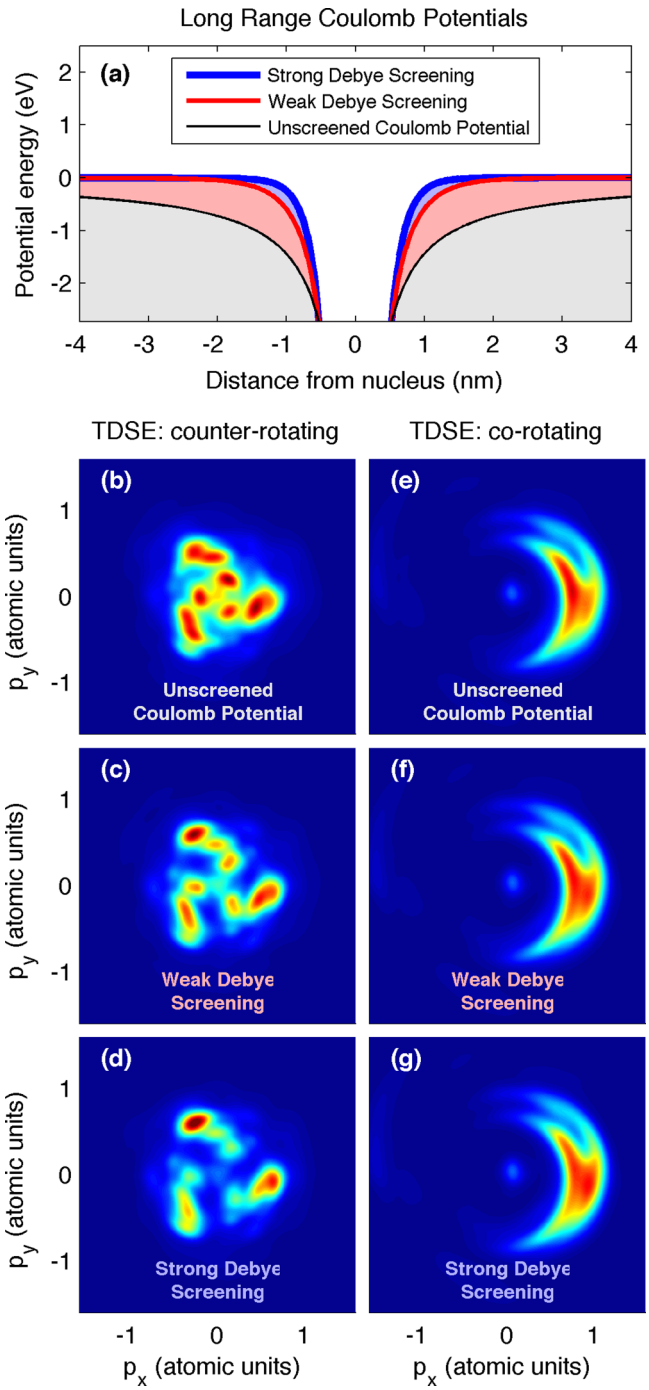

FIG. 4. (Color online) Time-dependent Schrödinger equation (TDSE) simulations investigating the effects of the Coulomb potential. (a) The electron-nuclear potentials used in the TDSE calculations. (b)–(d) For the counter-rotating case, the low-energy structures disappear as the screening factor for the Coulomb potential is increased, confirming that the low-energy structures are due to strong electron-ion rescattering. (e)–(g) In the co-rotating case there is no change as the screening factor is varied, indicating the absence of rescattering.

any effect of the Coulomb potential of the parent ion. The SFA adequately reproduces the co-rotating case. However, for the counter-rotating case, the SFA model matches the symmetry and the kinetic energy of the experimental photoelectron distributions, but there is a significant difference: the experimental photoelectron distribution has a low-energy structure that is not captured by the simple model. The absence of this structure from the model suggests that it is a result of the interaction between the Coulomb potential of the parent ion and the returning electrons.

To further understand how the low-energy structures depend on the Coulomb potential, the 3D time-dependent Schrödinger equation (TDSE) is solved using a generalized pseudospectral method [47,48]. To isolate the effect of the Coulomb potential, we "turned off" the influence of the long-range Coulomb potential by adding a Debye screening factor starting at an electron-ion distance of $r = 10$ atomic units of the form $\exp[-(r-10)/r_a]$. The screening factor r_a was set at ∞, 10, and 5 atomic units, which corresponds to an unscreened Coulomb potential, a weakly screened Coulomb potential, and a strongly screened Coulomb potential, respectively [Fig. 4(a)]. The simulations assume an intensity of 5×10^{13} W cm^{-2} for each color.

The simulated photoelectron distributions are in very good agreement with the experimental data, reproducing the energies, symmetries, and general shape of the photoelectron distributions for both the co- and counter-rotating fields. In the case of the co-rotating fields [Figs. 4(e)–4(g)], there is little effect observed from varying the screening of the Coulomb potential, indicating that the tunnel-ionized electrons are not driven back near the parent ion. However, for the counter-rotating field [Figs. 4(b)–4(d)], the inner structures are strongly influenced by the presence of the Coulomb potential, confirming that the laser field drives the electrons in close proximity to the ion.

In summary, we made observations of the 3D photoelectron distributions resulting from the strong-field ionization by two-color circularly polarized laser fields, providing experimental validation for the theory of high-harmonic generation in this important regime. We found that the general shape and symmetry of the photoelectron distributions is well explained by a simple strong-field model, which ignores the Coulomb potential of the ion. However, in the case of counter-rotating two-color fields, we observed low-energy structures in the photoelectron distribution, indicating the presence of electron-ion rescattering. Numerical simulations using the time-dependent Schrödinger equation confirm that the Coulomb potential is responsible for the appearance of the low-energy electrons. Importantly, both the experiment and theory indicate that the rescattered electrons are well separated in energy from those electrons that do not re-encounter the ion, indicating that strong-field ionization using these complex polarization-shaped fields may lead to breakthrough techniques for studying atomic and molecular dynamics.

The experimental work was done at JILA, with funding from the US Department of Energy Office of Basic Energy Sciences AMOS program and from the Physics Frontiers Center. JILA also gratefully acknowledges support from an AFOSR DURIP award for the laser system used for this work. C.A.M. acknowledges support from the National Science Foundation Graduate Research Fellowship under Grant No. DGE 1144083. P.G. acknowledges support from the Deutsche Forschungsgemeinschaft Grant

No. GR 4234/1–1. R.K. acknowledges the Swedish Research Council (VR) for their financial support. This work was supported by the USA-Israel Binational Science Foundation (BSF). O.K. was supported by the Prof. Rahamimoff Travel Grant for Young Scientists through the BSF, Grant No. T-2014-118. The Technion group was supported by the Israel Science Foundation, Grant No. 1225/14, and the Israeli Center of Research Excellence "Circle of Light" supported by the I-CORE Program. X.M.T. was supported by a Grant-in-Aid for Scientific Research (Grant No. C24540421) from the JSPS and the HA-PACS Project for advanced interdisciplinary computational sciences by exa-scale computing technology. X.M.T. thanks Prof. K. Yabana for helpful discussions.

APPENDIX: TIME-DELAY TDSE SIMULATIONS

In order to confirm the experimentally observed time-dependent photoelectron distributions [Figs. 2(c) and 2(d)], we undertook TDSE simulations [47,48] using various time delays of the laser pulses. The photoelectron distributions from the TDSE simulations were obtained using two different conditions: (1) a 60-fs scan with 0.5-fs steps [Figs. 5(a) and 5(b)] and (2) a 3.2-fs scan with 0.1-fs steps [Figs. 5(c) and 5(d)]. The 60-fs scan reveals the change in the photoelectron yield due to the cross-correlations between the two laser pulses, and both cases reveal oscillations every 1.33 fs. In the co-rotating case, a majority of the photoelectrons in the co-rotating case are driven to higher-kinetic energies, whereas the counter-rotating fields produce significantly lower energy electrons. This agrees well with the experimental data shown in Figs. 2(c) and 2(d).

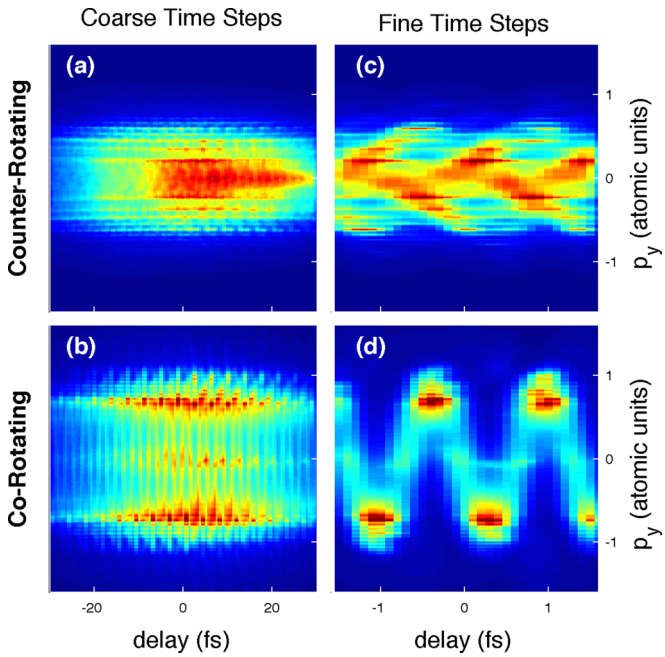

FIG. 5. (Color online) (a),(b) Coarse time step TDSE simulations reveal the change in the photoelectron yield due to the cross-correlations between the two laser pulses, and oscillations every 1.33 fs. In the co-rotating case, most of the electrons are driven to higher-kinetic energies, whereas a large number of low-energy electrons can be seen in the counter-rotating case. (c),(d) Fine time-step TDSE simulations show good agreement with the experimentally observed sinograms presented in Figs. 2(c) and 2(d).

[1] A. Mcpherson, G. Gibson, H. Jara, U. Johann, T. S. Luk, I. A. Mcintyre, K. Boyer, and C. K. Rhodes, Studies of multiphoton production of vacuum-ultraviolet radiation in the rare gases, J. Opt. Soc. Am. B **4**, 595 (1987).

[2] P. Agostini, F. Fabre, G. Mainfray, G. Petite, and N. K. Rahman, Free-free transitions following six-photon ionization of xenon atoms, Phys. Rev. Lett. **42**, 1127 (1979).

[3] D. D. Hickstein, P. Ranitovic, S. Witte, X.-M. Tong, Y. Huismans, P. Arpin, X. Zhou, K. E. Keister, C. W. Hogle, B. Zhang, C. Ding, P. Johnsson, N. Toshima, M. J. J. Vrakking, M. M. Murnane, and H. C. Kapteyn, Direct visualization of laser-driven electron multiple scattering and tunneling distance in strong-field ionization, Phys. Rev. Lett. **109**, 073004 (2012).

[4] T. Popmintchev, M.-C. Chen, P. Arpin, M. M. Murnane, and H. C. Kapteyn, The attosecond nonlinear optics of bright coherent X-ray generation, Nat. Photonics **4**, 822 (2010).

[5] X. Zhou, P. Ranitovic, C. W. Hogle, J. H. D. Eland, H. C. Kapteyn, and M. M. Murnane, Probing and controlling non-Born-Oppenheimer dynamics in highly excited molecular ions, Nat. Phys. **8**, 232 (2012).

[6] E. Gagnon, P. Ranitovic, X.-M. Tong, C. L. Cocke, M. M. Murnane, H. C. Kapteyn, and A. S. Sandhu, Soft x-ray-driven femtosecond molecular dynamics, Science **317**, 1374 (2007).

[7] W. Li, X. Zhou, R. Lock, S. Patchkovskii, A. Stolow, H. C. Kapteyn, and M. M. Murnane, Time-resolved dynamics in N_2O_4 probed using high harmonic generation, Science **322**, 1207 (2008).

[8] C. La-O-Vorakiat, M. Siemens, M. M. Murnane, H. C. Kapteyn, S. Mathias, M. Aeschlimann, P. Grychtol, R. Adam, C. M. Schneider, J. M. Shaw, H. Nembach, and T. J. Silva, Ultrafast demagnetization dynamics at the M edges of magnetic elements observed using a tabletop high-harmonic soft x-ray source, Phys. Rev. Lett. **103**, 257402 (2009).

[9] C. La-O-Vorakiat, E. Turgut, C. A. Teale, H. C. Kapteyn, M. M. Murnane, S. Mathias, M. Aeschlimann, C. M. Schneider, J. M. Shaw, H. T. Nembach, and T. J. Silva, Ultrafast demagnetization measurements using extreme ultraviolet light: Comparison of electronic and magnetic contributions, Phys. Rev. X **2**, 011005 (2012).

[10] K. M. Hoogeboom-Pot, J. N. Hernandez-Charpak, X. Gu, T. D. Frazer, E. H. Anderson, W. Chao, R. W. Falcone, R. Yang, M. M. Murnane, H. C. Kapteyn, and D. Nardi, A new regime of nanoscale thermal transport: Collective diffusion increases dissipation efficiency, Proc. Natl. Acad. Sci. USA, doi:10.1073/pnas.1503449112.

[11] M. D. Seaberg, D. E. Adams, E. L. Townsend, D. A. Raymondson, W. F. Schlotter, Y. Liu, C. S. Menoni, L. Rong, C.-C. Chen, J. Miao, H. C. Kapteyn, and M. M. Murnane, Ultrahigh 22 nm resolution coherent diffractive imaging using a desktop 13 nm high harmonic source, Opt. Express **19**, 22470 (2011).

[12] R. L. Sandberg, A. Paul, D. A. Raymondson, S. Hädrich, D. M. Gaudiosi, J. Holtsnider, R. I. Tobey, O. Cohen, M. M. Murnane, H. C. Kapteyn, C. Song, J. Miao, Y. Liu, and F.

Salmassi, Lensless diffractive imaging using tabletop coherent high-harmonic soft-x-ray beams, Phys. Rev. Lett. **99**, 098103 (2007).

[13] C. I. Blaga, J. Xu, A. D. DiChiara, E. Sistrunk, K. Zhang, P. Agostini, T. A. Miller, L. F. DiMauro, and C. D. Lin, Imaging ultrafast molecular dynamics with laser-induced electron diffraction, Nature (London) **483**, 194 (2012).

[14] J. Xu, Z. Chen, A.-T. Le, and C. D. Lin, Self-imaging of molecules from diffraction spectra by laser-induced rescattering electrons, Phys. Rev. A **82**, 033403 (2010).

[15] J. Xu, C. I. Blaga, K. Zhang, Y. H. Lai, C. D. Lin, T. A. Miller, P. Agostini, and L. F. DiMauro, Diffraction using laser-driven broadband electron wave packets, Nat. Commun. **5**, 4635 (2014).

[16] W. Li, A. A. Jaroń-Becker, C. W. Hogle, V. Sharma, X. Zhou, A. Becker, H. C. Kapteyn, and M. M. Murnane, Visualizing electron rearrangement in space and time during the transition from a molecule to atoms, Proc. Natl. Acad. Sci. USA **107**, 20219 (2010).

[17] P. B. Corkum, Plasma perspective on strong field multiphoton ionization, Phys. Rev. Lett. **71**, 1994 (1993).

[18] P. Dietrich, N. H. Burnett, M. Ivanov, and P. B. Corkum, High-harmonic generation and correlated two-electron multiphoton ionization with elliptically polarized light, Phys. Rev. A **50**, R3585(R) (1994).

[19] F. A. Weihe, S. K. Dutta, G. Korn, D. Du, P. H. Bucksbaum, and P. L. Shkolnikov, Polarization of high-intensity high-harmonic generation, Phys. Rev. A **51**, R3433(R) (1995).

[20] Y. Huismans, A. Rouzée, A. Gijsbertsen, J. H. Jungmann, A. S. Smolkowska, P. S. W. M. Logman, F. Lépine, C. Cauchy, S. Zamith, T. Marchenko, J. M. Bakker, G. Berden, B. Redlich, A. F. G. van der Meer, H. G. Muller, W. Vermin, K. J. Schafer, M. Spanner, M. Y. Ivanov, O. Smirnova, D. Bauer, S. V. Popruzhenko, and M. J. J. Vrakking, Time-Resolved holography with photoelectrons, Science **331**, 61 (2011).

[21] C. T. L. Smeenk, L. Arissian, B. Zhou, A. Mysyrowicz, D. M. Villeneuve, A. Staudte, and P. B. Corkum, Partitioning of the linear photon momentum in multiphoton ionization, Phys. Rev. Lett. **106**, 193002 (2011).

[22] J. Küpper, Strong-field physics: Displaced creation, Nat. Phys. **10**, 550 (2014).

[23] M. Meckel, A. Staudte, S. Patchkovskii, D. M. Villeneuve, P. B. Corkum, R. Dörner, and M. Spanner, Signatures of the continuum electron phase in molecular strong-field photoelectron holography, Nat. Phys. **10**, 594 (2014).

[24] D. Shafir, Y. Mairesse, D. M. Villeneuve, P. B. Corkum, and N. Dudovich, Atomic wavefunctions probed through strong-field light-matter interaction, Nat. Phys. **5**, 412 (2009).

[25] A. Fleischer, O. Kfir, T. Diskin, P. Sidorenko, and O. Cohen, Spin angular momentum and tunable polarization in high-harmonic generation, Nat. Photonics **8**, 543 (2014).

[26] C. I. Blaga, F. Catoire, P. Colosimo, G. G. Paulus, H. G. Muller, P. Agostini, and L. F. DiMauro, Strong-field photoionization revisited, Nat. Phys. **5**, 335 (2009).

[27] F. H. M. Faisal, Strong-field physics: Ionization surprise, Nat. Phys. **5**, 319 (2009).

[28] C. Liu and K. Z. Hatsagortsyan, Origin of unexpected low energy structure in photoelectron spectra induced by mid-infrared strong laser fields, Phys. Rev. Lett. **105**, 113003 (2010).

[29] T.-M. Yan, S. V. Popruzhenko, M. J. J. Vrakking, and D. Bauer, Low-energy structures in strong field ionization revealed by quantum orbits, Phys. Rev. Lett. **105**, 253002 (2010).

[30] C. Lemell, K. I. Dimitriou, X.-M. Tong, S. Nagele, D. V. Kartashov, J. Burgdörfer, and S. Gräfe, Low-energy peak structure in strong-field ionization by midinfrared laser pulses: Two-dimensional focusing by the atomic potential, Phys. Rev. A **85**, 011403(R) (2012).

[31] D. B. Milošević, W. Becker, and R. Kopold, Generation of circularly polarized high-order harmonics by two-color coplanar field mixing, Phys. Rev. A **61**, 063403 (2000).

[32] D. B. Milošević and W. Becker, Attosecond pulse trains with unusual nonlinear polarization, Phys. Rev. A **62**, 011403(R) (2000).

[33] H. Eichmann, A. Egbert, S. Nolte, C. Momma, B. Wellegehausen, W. Becker, S. Long, and J. K. McIver, Polarization-dependent high-order two-color mixing, Phys. Rev. A **51**, R3414(R) (1995).

[34] O. Kfir, P. Grychtol, E. Turgut, R. Knut, D. Zusin, D. Popmintchev, T. Popmintchev, H. Nembach, J. M. Shaw, A. Fleischer, H. Kapteyn, M. Murnane, and O. Cohen, Generation of bright phase-matched circularly-polarized extreme ultraviolet high harmonics, Nat. Photonics **9**, 99 (2015).

[35] E. Pisanty, S. Sukiasyan, and M. Ivanov, Spin conservation in high-order-harmonic generation using bicircular fields, Phys. Rev. A **90**, 043829 (2014).

[36] N. Böwering, T. Lischke, B. Schmidtke, N. Müller, T. Khalil, and U. Heinzmann, Asymmetry in photoelectron emission from chiral molecules induced by circularly polarized ligth, Phys. Rev. Lett. **86**, 1187 (2001).

[37] A. Ferré, C. Handschin, M. Dumergue, F. Burgy, A. Comby, D. Descamps, B. Fabre, G. A. Garcia, R. Géneaux, L. Merceron, E. Mével, L. Nahon, S. Petit, B. Pons, D. Staedter, S. Weber, T. Ruchon, V. Blanchet, and Y. Mairesse, A table-top ultrashort light source in the extreme ultraviolet for circular dichroism experiments, Nat. Photonics **9**, 93 (2015).

[38] G. Schütz, M. Knülle, and H. Ebert, Magnetic circular x-ray dichroism and its relation to local moments, Phys. Scr. **T49A**, 302 (1993).

[39] A. T. J. B. Eppink and D. H. Parker, Velocity map imaging of ions and electrons using electrostatic lenses: Application in photoelectron and photofragment ion imaging of molecular oxygen, Rev. Sci. Instrum. **68**, 3477 (1997).

[40] M. Wollenhaupt, C. Lux, M. Krug, and T. Baumert, Tomographic reconstruction of designer free-electron wave packets, ChemPhysChem **14**, 1341 (2013).

[41] C. Smeenk, L. Arissian, A. Staudte, D. M. Villeneuve, and P. B. Corkum, Momentum space tomographic imaging of photoelectrons, J. Phys. B **42**, 185402 (2009).

[42] D. Dimitrovski, J. Maurer, H. Stapelfeldt, and L. B. Madsen, Low-energy photoelectrons in strong-field ionization by laser pulses with large ellipticity, Phys. Rev. Lett. **113**, 103005 (2014).

[43] G. N. Hounsfield, Computerized transverse axial scanning (tomography): Part 1. Description of system, Br. J. Radiol. **46**, 1016 (1973).

[44] V. Dribinski, A. Ossadtchi, V. A. Mandelshtam, and H. Reisler, Reconstruction of Abel-transformable images: The Gaussian basis-set expansion Abel transform method, Rev. Sci. Instrum. **73**, 2634 (2002).

[45] See Supplemental Material at http://link.aps.org/supplemental/10.1103/PhysRevA.91.031402 for videos that show the rotation of (1) the electric field and final drift momentum and (2) the photoelectron distributions detected with the velocity map imaging spectrometer.

[46] A. C. Kak and M. Slaney, *Principles of Computerized Tomographic Imaging* (IEEE, New York, 1988).

[47] X. M. Tong, K. Hino, and N. Toshima, Phase-dependent atomic ionization in few-cycle intense laser fields, Phys. Rev. A **74**, 031405(R) (2006).

[48] X.-M. Tong and Shih-I. Chu, Generation of circularly polarized multiple high-order harmonic emission from two-color crossed laser beams, Phys. Rev. A **58**, R2656(R) (1998).